Master of Science Thesis

Intrafractional prostate movement studied by electronic portal imaging in cine mode

Torbjörn Månsson Haskå

Supervisor:
[1]Henriette Honoré PhD, [1]Per Rugård Poulsen PhD and Tommy Knöös PhD

[1]Medical Radiation Physics,
Århus University Hospital

Medical Radiation Physics
Clinical Sciences, Lund
Lund University, 2006

Introduction: This thesis is a study of the margins that are necessary in prostate cancer radio therapy treatment. The aim was to analyse the intrafraction motion of the prostate gland during treatment, by the use of portal imaging, in order to optimize the margin around the prostate gland and spare healthy tissue. One of the purposes was to find a common pattern in prostate movement in the first fractions of the treatment that could describe the movement during the following fractions. The intention was to create individual margins for each patient for the rest of the treatment. Further analyses of the portal images were made to visualize the directions and size of the prostate gland motion in order to reduce the planning target volume (PTV) already from the first treatment.

Materials and Methods: Twenty patients with diagnosed prostate cancer had three gold seed markers inserted in the prostate gland. A five field forward planned step-and-shoot technique was used for the treatment. The gantry angles used were 180°, 103°, 36°, 257° and 324°. For all patients CINE picture sequences were recorded with the electronic portal imaging devices (EPID) during fractions 2, 3, 4, 9, 14, 19, 24, 29, 34, and 39. On five of the patients a full analysis was performed which consisted of an analysis of all CINE pictures recorded. It was done in order to visualize the magnitude of the motion of the prostate in the three directions lateral (LT), cranial-caudal (CC) and posterior-anterior (PA). On fifteen patients a reduced analysis was performed which contained an analysis of the first CINE picture for each field. This was done in order to visualize the magnitude of the motion of the prostate gland motion in the CC direction. The image analysis was performed in two computer software programs: Image J and Microsoft Excel. A accelerator arm sag measurement was performed on the three different accelerators that were used for treatment. The results of these measurements were used to correct the CC analysis and to estimate a correction factor that could be used in the PA analysis.

Results: There was no common pattern found that could describe the intrafraction motion of the prostate gland during the treatment. A specificity and sensitivity analysis showed that it is possible to predict only two thirds of all cases. The results from the full analysis showed that there were only small intrafield displacements (< 1 mm) relative to the intrafraction displacements which were much larger, in some cases several mm. The results from the two analyses showed that there was a correlation in the motion of the prostate gland in the cranial-anterior direction and in the caudal-posterior direction. For one patient the squared correlation factor was 0.75. The size of the motion never exceeded 7 mm in the CC direction, 95 % of all fractions had a maximum motion of < 4.1 mm in the CC direction and 98 % of all *field 1*'s were < 1.0 mm in the LT direction. No exact results for the anterior-posterior direction were reached.

Conclusions: There were 196 fractions analysed and in 95% of these a deviation of < 4.1 mm in CC direction was observed. An increased mean displacement relative the start position was shown for fields 1, 2, 3 and 4 and then it looks like a steady state was reached. In most cases the maximum displacement in each fraction occurred in field 4. These results imply that the motion of the prostate gland probably reaches a steady state with time. Intrafractional and intrafield motion of the prostate gland is not possible to predict, it can occur in any fraction during treatment and often in combination with gas in the rectum.

Supervisors: **Henriette Honoré PhD** and **Per Rugård Poulsen PhD** Medical Radiation Physics, Århus University Hospital, **Tommy Knöös PhD** Medical Radiation Physics, Lund University Hospital
Degree project 20 credits in Medical Radiation Physics, Autumn 2006
Department of Medical Radiation Physics, Lund University

Introduction

Aim

This thesis is a study of the margins that are necessary in prostate cancer radiotherapy treatment. The aim was to analyse the prostate motion during treatment by the use of portal imaging in order to optimize the margin around the prostate gland and spare healthy tissue.

External radiotherapy

External radiation therapy is one of the most common treatments of prostate cancer along with surgery, chemotherapy and internal radiotherapy. In some cases a combination of two or more treatment methods are to prefer in order to get the best treatment outcome. The goal with radiotherapy is to get a satisfying dose distribution with maximum tumour control and the lowest possible level of side effects [6]. If it is possible to use tight safety margins around the target, it would possibly enable high tumour control with few side effects. The limitation for reducing the margin is organ motions and set-up errors [7]. For prostate cancer treatment with external radiotherapy, dose escalation has shown to give an increased tumour control [10]. Doses of 78 Gy or higher is necessary for the best possible outcome of the treatment [9]. The newest techniques in 3D conformal radio therapy (CRT) with multileaf collimators (MLC) and intensity modulated radiotherapy (IMRT) give the possibility to shape the dose distribution as desired while maintaining an acceptable level of side effects [11]. Reducing the margin is important in order to spare the surrounding organs at risk and to make dose escalation possible [8, 12].

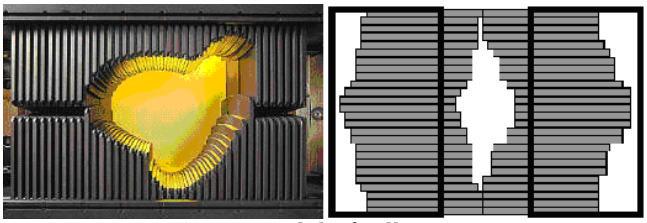

Figure.1 Multileaf collimator [1]

Volume definitions

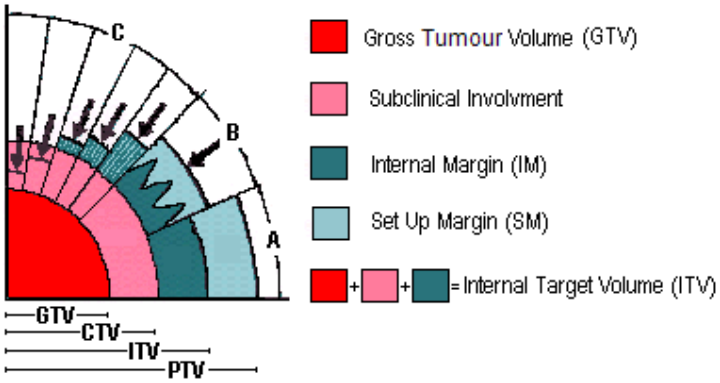

Figure.2 Volume definitions according to ICRU 50 and ICRU 62

Computerized tomography (CT) based target delineation has become a very important part of the treatment planning process. The three dimensional anatomy map of the electron density is used to

accurately outline the target volume and organs of interest in all relevant CT-slices. ICRU 50 and ICRU 62 (1999) describe and define the procedure of drawing the different target volumes. The gross tumour volume (GTV) is the part of the tumour that is the gross, palpable, visible or clinically demonstrable location and extent of the malignant growth. The clinical target volume (CTV) includes the GTV plus a margin that takes into account a potential microscopic tumour-cell infiltration of the healthy tissue. If there is a spread to the lymphatic system it should also be included in the CTV.

In example **A** (figure 2) the internal target volume (ITV) is the CTV and an internal margin (IM) that takes into account organ motion and any change in shape and size. The planning target volume (PTV) includes the CTV and IM plus a set-up margin (SM) that takes into account the variation and uncertainties in patient positioning from day to day. Information about organ motion can be found in studies like the present or in the literature [15]. The information about the set up uncertainties is to be found locally as they are dependent of the particular modalities, staff and routines of a clinic. Example **A** is illustrating a theoretical PTV where the different margins are added linearly and result in a very large PTV. This kind of PTV is not often used in the clinic since it results in unrealistically large margins.

In example **B (**figure 2) the PTV includes the CTV plus in some cases a small IM and a large SM or vice versa. In this example it is assumed that some of the errors caused by internal motion and set up inaccuracy cancel each other and the PTV is therefore reduced. This could spare the healthy tissue and provide fewer side effects.

In example **C** (Figure 2) there are five illustrations that show the use of individual treatment situations. For example the PTV margin should be reduced to a minimum if the tumour is too close to an organ at risk (OAR) or/and if there is a possibility to spare some of the functions of the radiated organ. An example could be prostate cancer where the prostate gland is close to the rectum wall and the urinary bladder - both which are considered as OARs, or lung tumours where it is in some cases possible to spare the healthy part of the organ to give a better quality of life for the patient post treatment. Another example is palliative treatment where it is often of less importance to spare the surroundings of minimizing the late effects. When using the PTV illustrated in **B** and **C** careful considerations have to be taken and should be discussed between the physicist and the oncologist in order to reach the best outcome of the treatment.

The *treated volume* is the volume enclosed by an iso-dose surface selected and specified by the radiation oncologist as appropriate to achieve the purpose of treatment (e.g. 95% iso-dose surface). The volume that receives a high dose relative to normal tissue tolerance is the irradiated volume. The aim of the treatment planning is typically to enclose PTV within the 95% isodose line. The 95% isodose line is the boundary where the dose is 95% of the prescribed dose.

In order to reduce the margins in the three directions (LT, CC, PA) it is necessary to have access to guidance imaging equipment and all the uncertainties through the procedure have to be accounted for.

On-board kV imager (OBI) and the gold seed marker

It is difficult to visualize the prostate gland on X-ray images due to the small attenuation differences between soft tissues. The problem can be solved by implanting radiopaque markers which are used as surrogates for the position of the prostate gland. There are other possibilities to visualize or localize the prostate gland using the on-board imager (OBI) modalities, e.g. the rectal balloon [16], the thermo-expandable stent [17] or the urethral catheter containing radiopaque markers [18, 19]. Another technique used to visualize the prostate gland without using radiopaque markers is cone beam computerized tomography (CBCT). A CBCT is a volumetric imaging of the pelvis and it can be matched to the planning CT scan. For example the bony structure could be used to make a 3D match. The advantage of the 3D match compared to the 2D match (with OBI, digital reconstructed radiographs (DRR) and gold seed markers) is the accuracy and the possibility to see the daily volume changes of CTV and OAR. A disadvantage is that it is time consuming. One scan and the following reconstruction with a CBCT take approximately 6 min, while using the method of OBI and DRR for set up only takes 4 min.

The gold seed marker has improved the efficacy and accuracy in radiation therapy for prostate gland cancer. The size of the marker is 3 mm in length and 1.2 mm in diameter. All three gold seed markers are placed into the prostate gland during transrectal surgery guided by ultrasound. One marker is inserted to the right and ~1/3 from the top of the prostate so there will be no risk that the marker is placed in the bladder by mistake, marker two is placed to the left and ~2/3 from the top and the third marker is inserted in the apex of the prostate. The gold seed markers are used with the accelerator modalities to reduce the inaccuracy of the set-up procedure. They are visualized through imaging devices, for example an electronic portal imaging device (EPID) or OBI. In the images the gold seed markers are clearly visible. Using the three gold seed markers the OBI images are then matched with the DRR from the CT scan in order to make couch adjustments to get the prostate in correct position for treatment. Studies have indicated that the markers do not move significantly within the prostate during or between treatments to affect the accuracy in treatment set ups [13, 14].

Figure 3. CINE image with three gold seed markers

The following is an example of the daily treatment set up using the gold seed markers at Aarhus University hospital:
To position the prostate before the daily treatment the OBI and the DRR are used. The gold seed markers are clearly visible in both the anterior and the lateral (LT) OBI images. Computer software is used to match the two images and to calculate the couch shift in order to get the correct prostate in position.

Cine image

A CINE image is a portal MV imaging sequence recorded continuously during beam delivery. An image is taken every 0.75 seconds during the radiation session of one field using the accelerator beam and an electronic portal imaging device (EPID).

The focus of the thesis

This thesis focuses on external radiotherapy and the margins used in prostate cancer treatment. The tools that have been used are the CINE-image sequences recorded during the treatment of patients and two computer software programs for image analysis and calculations. It is known that the prostate gland (CTV) moves between fractions (interfraction motion) and during a fraction (intrafraction motion). To compensate for this a CTV to PTV margin is added. The purpose was to measure the organ motion in the first three fractions and then see if the results from these first fractions were representative for describing the organ motion in the following fractions. The next thing was to find out in what direction(s) the prostate gland was moving and if there was a pattern that could describe the motion. In this way it was possible to achieve information about the magnitude of the motion in the three directions: LT, CC and PA. Hopefully the results can be useful in the clinic to optimize the margins added to the CTV and thereby spare healthy tissue.

Prostate cancer

Today prostate cancer has become the most common cancer form in Sweden. In total 9882 men were diagnosed with prostate cancer in 2004 [2]. One reason for this increase in the number of cancer cases is the possibility to make an early diagnosis, mostly of non-palpable tumours (category T1c).

The prostate is a sex gland in men. It is about the size of a walnut, and surrounds the neck of the bladder and urethra. The secretes from the prostate gland gives nourishment to the male sperm and its growth and function is controlled by testosterone.

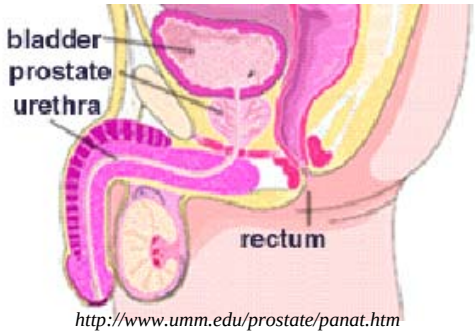

http://www.umm.edu/prostate/panat.htm

Figure 4. Anatomic position of the prostate.

Symptoms that could indicate a change in the prostate are: weak urine flow, frequent urinating, difficulties to urinate or hold back urine, inability to urinate, pain or burning when urinating, blood in the urine or semen, nagging pain in the back, hips, or pelvis. These symptoms are often not seen until the cancer has spread to the outside of the prostate gland [3, 4]. To categorize the cancer and decide what treatment should be used the doctor uses T-staging, Gleason-grading and PSA test results. *T-stage* describes the size and location of the tumour [4]. *Gleason-grading* describes how aggressive the tumour is on the basis of how closely the cell from the biopsy looks like cells from normal tissue. *PSA (Prostate Specific Antigen)* is an

enzyme that is produced in the prostate by both healthy and cancerous cells. A small part of the antigen leaks into the blood and its concentration can be measured. A measurement of PSA is based on a simple blood test [4].

Exactly what causes cancer in the prostate gland is not completely understood but testosterone is thought to have a large influence on the development of the disease [4]. Other *contributing factors* to prostate cancer include age, race, diet, weight, obesity, environmental exposures, having a vasectomy, benign prostatic hyperplasia, sexually transmitted disease, family history of prostate cancer and genetic factors [4].

The treatment for prostate cancer should take into account the patient's general health, age, expected life span, personal preferences, expected effects of the treatment, stage and grade of the cancer. The most common treatment forms are surgery, radiotherapy and chemotherapy.

Methods and Materials

Forty-one patients with diagnosed with prostate cancer had three gold seed markers inserted into the prostate by surgery. Twenty were used for this analysis. Twenty-one of the 41 patients were excluded for different reasons: nine patients had the markers inserted so that it was impossible to separate them in the CINE pictures. Eight patients had six markers inserted instead of three because the first set of markers had been placed outside the prostate by mistake and were not usable for treatment setup. The last four patients did not complete the treatment on time.

A five field treatment technique (see below) was used. The patients were dose planned in Varian[1] Eclipse treatment planning software with a forward planning technique. In prostate cancer treatment the whole prostate gland is included in the GTV, which means that the GTV is the same as the CTV. The volumes that were delineated were GTV50 which includes prostate and the vesicular seminale, and GTV78 which consists of the prostate only. The GTV50 received 50 Gy / 25 fractions and GTV78 received a boost of additional 28 Gy / 14 fractions. The photon beam quality used was 15 MV. To create the PTV a margin was added to the GTV: 5 mm in LT, 7 mm in anterior-posterior (AP) and 9 mm in the CC

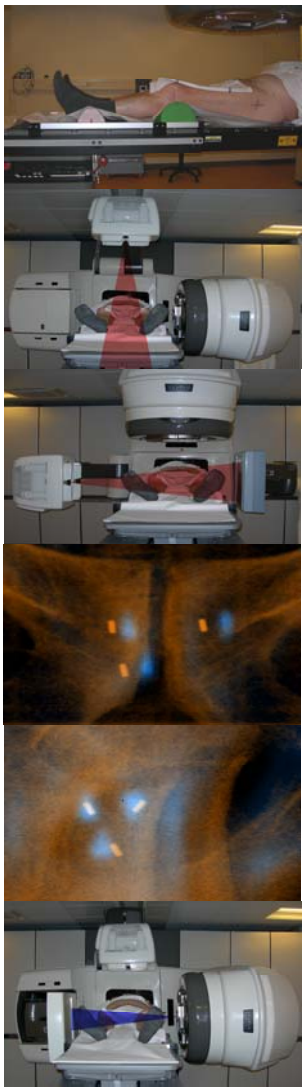

Figure 5a. Heel and knee fixation. **Figures 5b and 5c.** OBI imaging. **Figures 5d and 5e.** OBI-picture (orange) is matched to DRR-pictures (blue).**Figure 5f.** CINE pictures recorded.

[1] Varian Medical Systems, Incorporation of Palo Alto, California, USA

(CC) direction. A Varian Clinac 2100 with an on-board imager (OBI) was used for the daily set-up and treatment. The positioning procedure started with placing the patient on the couch in the same position as during the planning CT. External positioning aid such as heel and knee fixations, lasers and external skin marks are used to get the patient in the same position before each fraction. There are two kV images recorded from two orthogonal angels, at 0° and 270°. Using the three gold seed markers the two OBI images are then matched with the corresponding DRRs from the CT scan. Then the computer software calculates how much the couch has to be adjusted in the three directions LT, CC and PA in order to get the prostate in position. After adjustment the treatment fields were given. All patients had CINE pictures recorded during treatment for all five fields in fractions 2, 3, 4, 9, 14, 19, 24, 29, 34 and 39. An image was taken every 0.75 seconds with a Varian Clinac 2100 with an electronic portal imaging device (EPID). Two different EPIDs were used during this study: one Portal Vision AS 1000 EPID and two Portal Vision AS 500 EPID. When placed 150 cm from the linac source, they had a resolution in the ISO centre plane of 0.260 mm/pixel and 0.521 mm/pixel respectively. Radiation of one field takes approximately 10-15s depending on the number of monitor units delivered. In a movie sequence consisting of 13 to 20 pictures it is possible to see the motion of the prostate (gold seed markers) during the treatment.

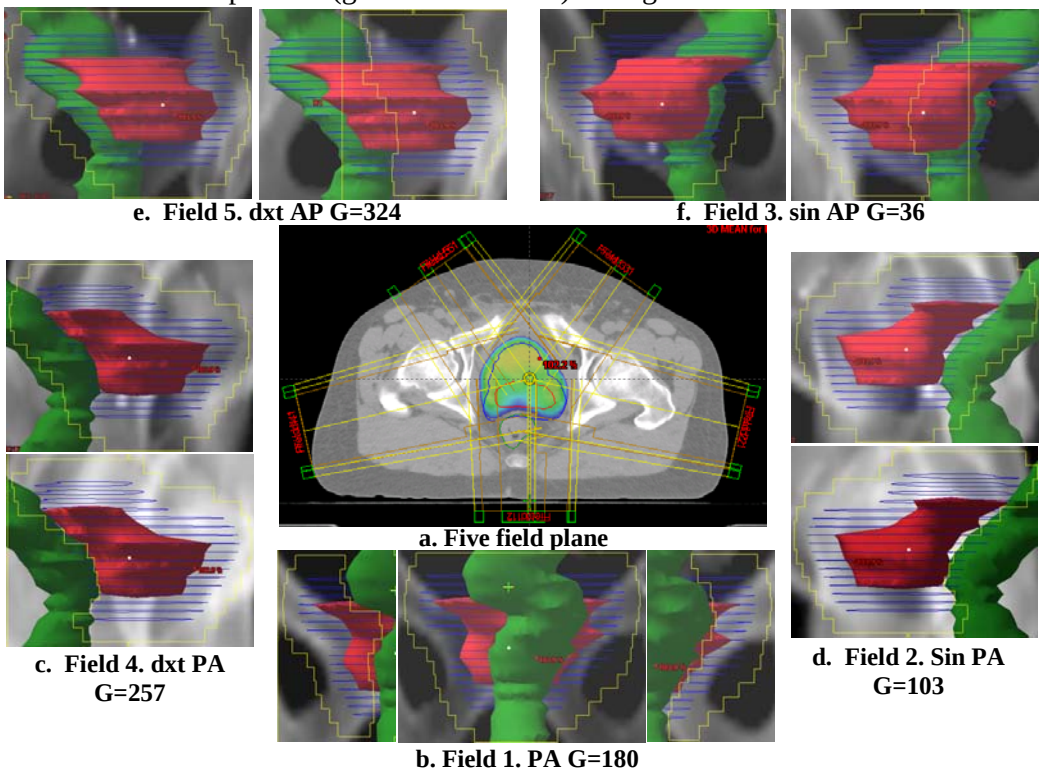

Figure 6a-f. Image **a** illustrates the five field technique. Images **b, c, d, e, f** show the primary field and the additional rectum shielding segment for each treatment angle. The red volume is the CTV, green volume is the rectum and the blue line is the PTV

The segmented forward planned five fields are delivered with a step-and-shoot technique. The five fields are visualized above. Each field starts with a primary segment which means that the whole PTV plus the margin are in the beam's eye view. Usually 80-90 % (62-70 Gy) of the mean PTV dose is delivered with the

primary segments. Then, segments are added with rectum shielding resulting in a PTV mean dose of 100 % (78 Gy). The present forward planned step-and-shoot technique is a treatment form with a conventional five field forward planned treatment plan with few segments. It is a less advanced technique than, e.g. inversely planned dynamic intensity modulated radiation therapy (IMRT). With the step-and-shoot technique the radiation beam stops while the multi-leaf collimator (MLC) changes from the shape of the primary segment to the shape of the rectum shielding segment. In dynamic IMRT the beam is on while the dynamic MLC changes form using a sliding window technique which means that the MLC changes form continuously to form the predetermined dose distribution to PTV. The difference between forward planned and inversely planned treatment is that the inverse planning starts with defining e.g. the minimum dose to the PTV and the maximum dose to the surrounding tissues and then the computer makes an optimization on those criteria. The forward plan is rather the opposite, with a manual trial and error procedure until the PTV minimum dose is reached and the surrounding tissues receive a dose as low as possible.

In the present study, five fields and their segments are delivered from five angles: 1-180°, 2-103°, 3-36°, 4-257° and 5-324°. All fields have one segment and one "shielding segment" except for field one which is delivered from a posterior direction (PA); it has two "shielding segments" to spare the rectum.

Dose restrictions:

- A minimum dose of 95% (74 Gy) delivered to the prostate (CTV)
- A minimum dose of 90% (70 Gy) delivered to the PTV
- A maximum of 1 cm^3 of the rectum is allowed a dose above 95 % (74 Gy)
- A maximum of 20 % of the rectum is allowed a dose above 90 % (70 Gy)
- Below 50 Gy to the circumference of the whole rectum

Analysis

The CINE images were analyzed in ImageJ [5], which is an image analysing freeware program, and in Microsoft Excel. The image analysis in ImageJ uses the function *Otsu Threshold* to outline the contour of the markers. The Otsu threshold is based on Otsu's algorithm which operates on the histogram of the image. A histogram is a probability distribution *p (g)*, which is the number of pixels n_g that has greyscale intensity *g* as a fraction of the total number of pixels *n*. The algorithm searches for the part of the histogram that has a minimum of overlap in the greyscale intensity distribution between the background and the region of interest (ROI). When the algorithm has set the threshold, the histogram is

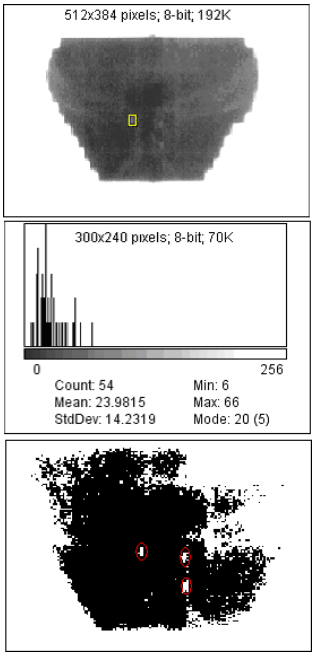

Figure 7a. CINE-picture with a selected area. **Figure 7b.** Histogram of the selected area. **Figure 7c.** The binary result of the Otsu threshold.

divided into two classes with a pixel value above and below the threshold, respectively. Pixels with a value above the threshold are set to 256 and pixels with a value below the threshold are set to 0. The outcome of this procedure is a binary image which shows the contour of the ROI. In ImageJ an image (small analysis) or sequence (full analysis) was opened one at the time. One of the gold seed markers was selected in the first image (Fig.7a) and the program was then used to calculate a threshold for the selected image/the whole image sequence for one of the five fields. In fig 7b the Otsu algorithm has set a threshold. When this procedure was completed the function *analyze particles* counted and measured the objects in the binary image (Fig.7c). In order to make a satisfactory calculation of the centre of mass for each marker (CM_m) it was necessary to have a sufficient number of pixels representing each marker. To get this number of pixels, two or three different threshold values were needed to outline the three markers in the CINE pictures. The *analyze particles* function works by scanning the image or selection until it finds the edge of an object and return the coordinates of the CM_m. At first the CM_m is of interest. The result from the Otsu threshold (Figure 7) is used to outline the seeds from the grey value of the original CINE picture. CM_m is a brightness weighted average of the x and y coordinates in the selected particle. The procedure is used to calculate the CM_m for each gold seed marker in each image of the sequence. Different thresholds were used to test if there was a variation in the position of the CM_m. The results showed a very small variation, smaller than the size of a pixel.

Full analysis

A full analysis was made on five of the patients. Of these five patients four were randomly selected and one was selected because of his large prostate motion during CINE imaging. The analysis consisted of a study of the position of the gold seed markers position in all portal images recorded during radiation of one fraction. In ImageJ an outline of the X and Y coordinates of the CM_m was made for all three markers. These were in the EPID image coordinate system. In Microsoft Excel they were converted into the treatment room coordinate system and the results were then plotted. Field 1 was set as a reference point to which the following four fields was related. This gives information of the motion of the markers for each field sequence and the motion in the whole fraction (see results). The direct result from the analysis shows a CC motion while a motion in the PA can not be determined directly. This is because the coordinates in the CC direction are independent of the gantry angle in contrast to the coordinates in the PA direction. To calculate the motion in the PA directions, it is necessary to make the assumption that there is no prostate motion in the LT directions. Furthermore the magnification factor and the field angles of the images must be known. In the PA field it was possible to detect that there was no LT motion during the approximately 10 seconds of radiation. The PA motion was calculated in Excel and the results could outline if there was a PA motion associated with the CC motion. The analysis could also give an indication of the approximate size of the PA motion.

The result from the full analysis shows that the motion of the prostate gland mostly occurred in between the recordings of the CINE images. One sequence lasted approximately 10 s and it took approximately 1 min to change gantry angle.

The CINE sequences only showed the intrafield motion that occurred during the approximately 50 s of radiation during a whole fraction which lasts for approximately 5 min. The full analysis was time consuming and gave practically the same results as the reduced analysis (described below) except for the intrafield information. The difference between the two analyses is that the full analysis included a larger amount of information about the prostate motion (because of a larger number of CINE pictures) than the reduced analysis.

Reduced analysis

The reduced analysis was used as an alternative way of calculating the intrafraction motion of the prostate gland. The first portal image of each field CINE sequence was selected for this smaller analysis and the remaining images in the CINE sequence were not used. The coordinates of the prostate centre of mass (CM) in the room coordinate system was calculated and plotted in Excel in the same way as in the full analysis. The plot shows the motion of the markers for one fraction in mm for fields 2 to 5 relative to field 1 (see results).

Cranial-Caudal (CC) analysis

Gantry arm sag correction

Before the coordinates from the ImageJ analysis could be used to calculate motions in the CC and the PA directions they had to be adjusted for the sag in the accelerator arm. To determine if the observed isocentre was angle dependent a five field standard plan for prostate treatment (see above) and a solid phantom were used. The phantom consists of five markers cast in a plastic cube. The cube was placed in the ISO-centre of the beam with the guidance of the external laser system in the treatment room. One portal image from each field angle was recorded and analysed in ImageJ. The cube and the four markers were fixed in the room coordinate system during the whole measurement procedure and were not affected by the five radiation angles. In this setup the only mobile part was the accelerator gantry including the EPID arm. The CM for the four markers as observed

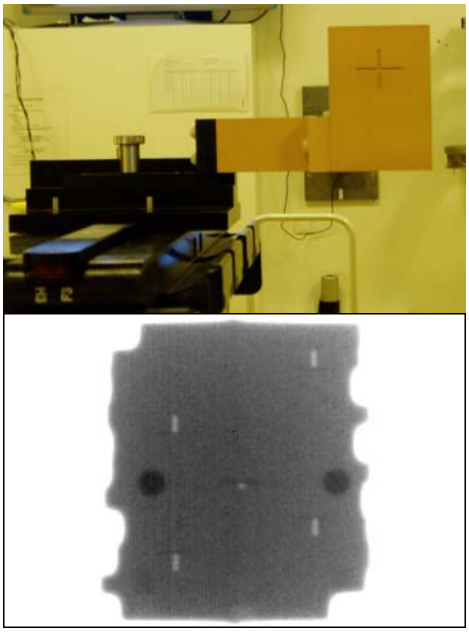

Figure 8a. Phantom fixed in the room's coordinate system. **Figure 8b.** EPID image with the four markers.

in the portal images were not in the same pixel of the EPID and the observed isocentre was therefore angle dependent. This was due to a sag in the accelerator arm. The sag is caused by the accelerator arm's own weight which means that the radiation beam is displaced from the isocentre. Sag is a system related error and can be corrected for. The calculation of the CM for the four markers was done in ImageJ and Excel in the same way as described above. The same procedure was made for the other accelerators used (5, 7 and 8). The results were then used to correct the results of the CC and PA analysis.

CC motion calculation

Using Excel, the centre of mass (CM) in each patient was calculated for all the three gold seed markers together. The Y coordinates of the CM_m representing the CC direction for the three individual markers in each image were added together and divided by three. This result thus represents the CM of the three markers. The positions of the markers in the prostate gland are assumed to be stable and thus the CM is assumed to represent the prostate motion [13, 14]. The coordinates for the CM for each image in each image sequence were calculated relative to the first image in the image sequence. This is visualized in a plot where the y-axis represents CC motion and the x-axis represents time (s) (plots 12 and 13). The results from all five fields in each fraction display the prostate motion during each radiation field as well as during the whole fraction.

Posterior-Anterior (PA) analysis

As mentioned earlier it is assumed that the prostate has only significant motion in CC and PA directions. In the portal image sequence of field one (PA-field), there are two types of prostate movements visible, one in the LT direction and one in the CC direction. One sequence lasts approximately 5-7s. An analysis of field one for the five patients (a total of 50 fractions) in the full analysis was made. If there was no notable motion (<1.0 mm) in LT direction it could be assumed that the prostate motion in LT direction was small and not significant. With this assumption it was possible to draw the conclusion that the only significant motion of the prostate was in the CC- and PA directions. For a certain movement in the PA direction the observed X coordinate in the portal images (X_{EPID}) was dependent of the field angle and a magnification factor (f). To get the information of the PA movement it was necessary to convert the coordinates from the portal image coordinate system (X_{EPID}, Y_{EPID}) to the room coordinate system (X_{Marker}, Y_{Marker}). The room coordinate system has its origin in the ISO centre of the target and is not moving with different gantry angles. The motion in PA direction was only visible in fields 2-5 and the calculated results are visualized in plots relative to field 2.

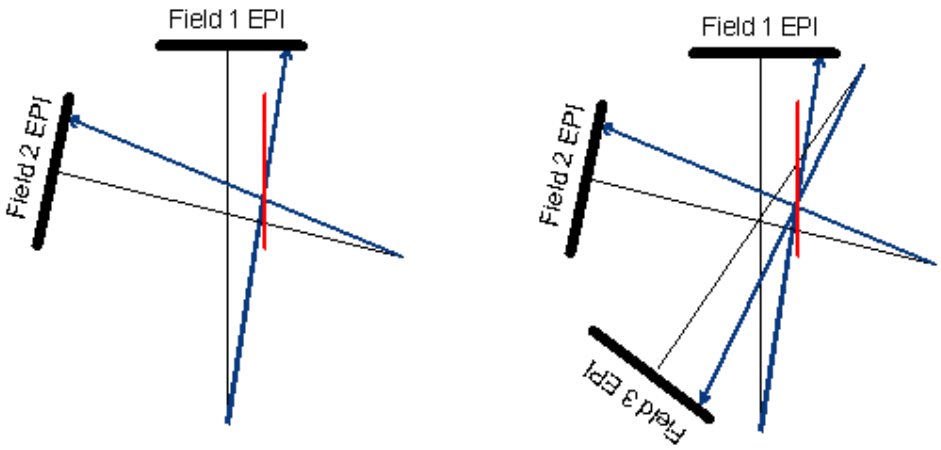

Figures 9a and 9b: The assessment of AP motion. The blue lines represent the projection of the marker into the EPID coordinate system. The red line represents the AP direction in the room coordinate system

The calculation of the PA position of the prostate gland in the room coordinate system started with defining the prostate gland position in field 1. By assuming that no motion in LT direction occurred between the images of fields 1 and 2 it was possible to calculate where the blue lines intersect in the room (figure 9a). The same calculation was made for fields 3, 4 and 5. If there was a displacement in between two fields it was assumed to be in direction of the red lines (figure 9b) due to the assumption of no LT motion.
The sag measurements of the stationary phantom were the basis for the calculation of the PA motion (see sag correction). The X-coordinates of the four markers from the analysis in ImageJ were in the EPID coordinate system (X_{EPID}). Each field is projected in the EPID coordinate system and was converted to the coordinate system of the room.

The equation for the AP calculation (see appendix)

Equation 4 in the appendix is a general equation with two unknown variables (X_{Marker}, Y_{Marker}). In equation 5 the field angle was set to 180° ($\alpha = 90$) which made it possible to isolate the unknown variable X_{Marker} (Eq.4 and 5). The new expression for X_{Marker} inserted in equation 4 gave a new equation (Eq.7) with only one unknown variable Y_{Marker}. In the last equation (Eq.9) the unknown variable Y_{Marker} was isolated and defined with known variables. In this way it was possible to calculate the position of the markers in the room coordinate from the EPID coordinates.

Correction factor calculation

There was a small displacement between the isocentres of the two coordinate systems that needed to be corrected. To convert the X_{EPID} to the X_{Marker} it was necessary to find an equation with a correction factor (Corr) that took in to account that the isocentre in the room was not projected in the isocentre of the image. It was possible to calculate the correction factor using equations 6 and 9 (see appendix). The coordinates in the room were calculated using the two equations and the results

from the phantom measurements of field one ($\alpha = 90$). Next, the expected EPID coordinates for fields 2, 3, 4 and 5 were calculated and the results were compared to the phantom measurements. The deviation of the calculated X_{EPID} and the measured X_{EPID} was squared and added. Using the *Excel solver function*, a correction factor was calculated, generating the smallest squared sum. In this way, the deviation between the expected and the measured X_{EPID} was minimized.

Results and discussion

CC-analysis

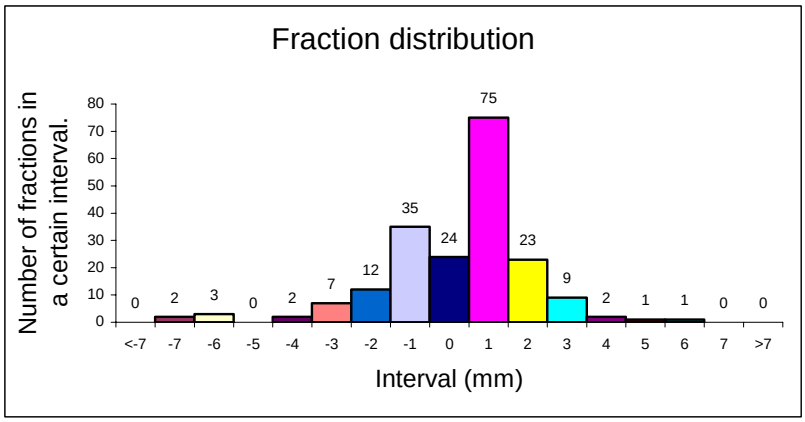

Figure 10. The distributions in CC direction of the 196 fractions analysed. A positive interval is in cranial direction and negative intervals in caudal direction

The most frequent displacements in the CC direction of the 196 analysed fractions were in the interval of 0.5-1.5 mm (Cranial direction). In contrast to what was expected, the distribution turned out to be non-symmetrical around zero, even after the results had been corrected for a sag in the accelerator arm (see below). It is probably due to a systematic error which could be related to the setup geometry.

Sag

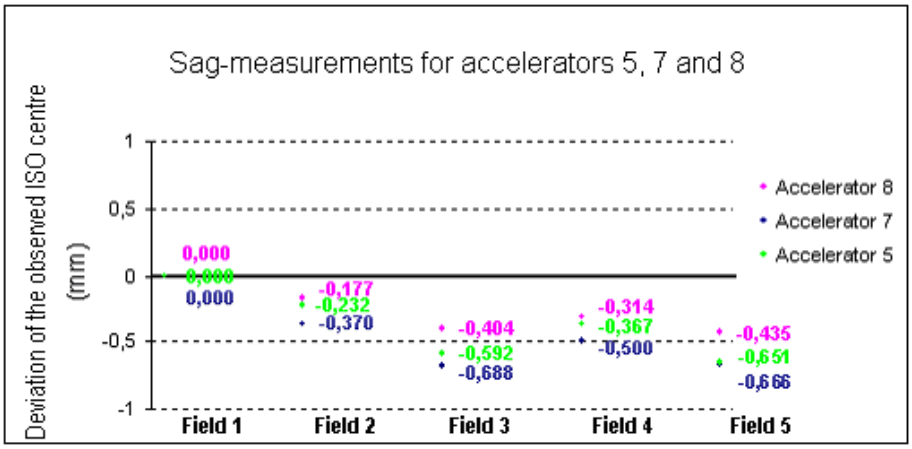

Figure 11. The results from the measurements of the sag in the accelerator arm for the five different field angles of accelerators 5, 7 and 8.

Figure 11 shows the ISO-centre deviation in mm for the five fields. The Y-axis represents the deviation from the start position of field 1. Along the X-axis the five fields are displayed. There was no time dependence in the measurements. The correction factor was used in the CC analysis to adjust the ImageJ results. A negative result represents a deviation in cranial direction, while a positive result represents a deviation in caudal direction.

CC calculation

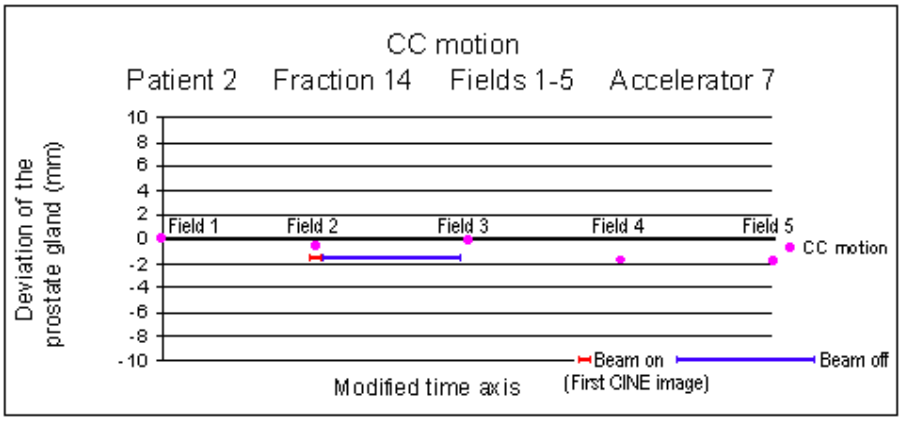

Figure 12. Example of the reduced analysis of the CC motion of the prostate gland. Each field is represented by a dot.

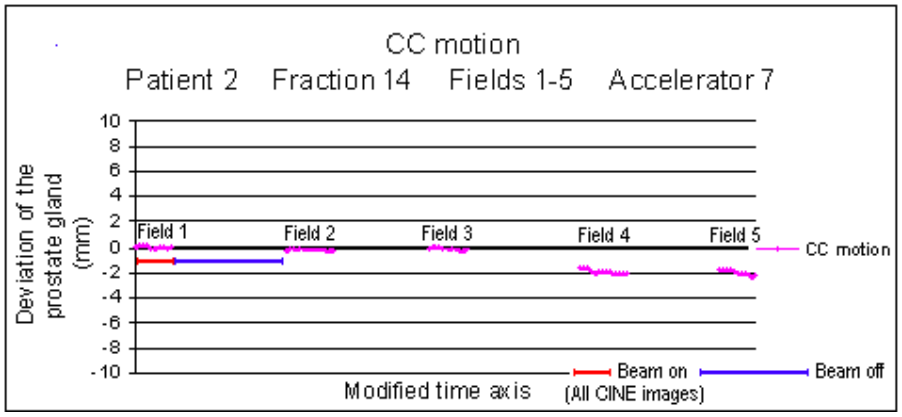

Figure 13. Example of the full analysis of the CC motion of the prostate gland. Each field is represented by a dot per CINE picture.

The plots show the results of the CC analysis for one fraction for one patient. Each mark represents a measurement and a calculation of the CINE picture/sequence (figures 12 and 13). The time axis between the fields has been truncated in order to save space and to better visualize the prostate gland motion. This means that the five fields are equally separated from each other in the plot. The results are inverted so that the motion in the cranial direction became positive and the motion in the caudal direction became negative.

Because there was no radiation between the fields there was no CINE picture recorded and it was not possible to get information about the motion of the prostate gland between the fields. After setup, one fraction took approximately 5 min to complete and each field took approximately 10 s to irradiate. The margin used in treatment planning in the CC direction was 9 mm because of the large motion in this direction. In this analysis motions as large as approximately 7.5 mm were noticed and other studies have reported even larger motions. In figure 14 it is possible to see which field that had the largest motion during all the treatments. In 75 of the 196 included fractions the largest motion occurred in field 4 which indicates that the deviation did not increase constantly. Instead it looks like it reaches a steady state and after a certain time interval the deviation does not increase with time. This result agrees with an unpublished study by Per Rugård Poulsen at Århus University hospital. He has studied the motion of the prostate gland between acquisition of the OBI set-up images and delivery of the first treatment field. The result shows that the motion is independent of the time interval between the images (time span 2-24 min). Considering this, it would be a good idea to reposition the prostate gland between field three and four in order to spare the surrounding tissue. Repositioning demands that the treatment is delivered at the same speed during all fractions and that there is no problem with the treatment equipment. As shown in figure 15, 95 % of all fractions had deviations less than 4.1 mm which could occur in both cranial and caudal direction.

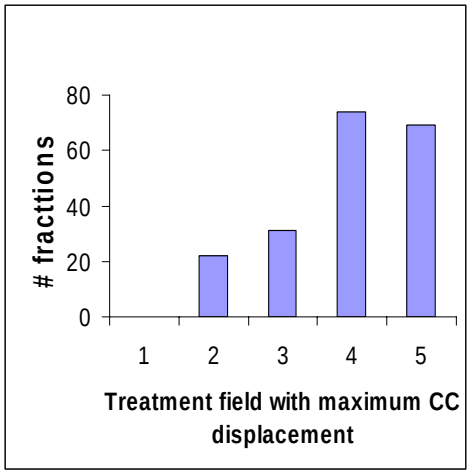

Figure 14. Shows in which field the maximum deviation in most cases occurred

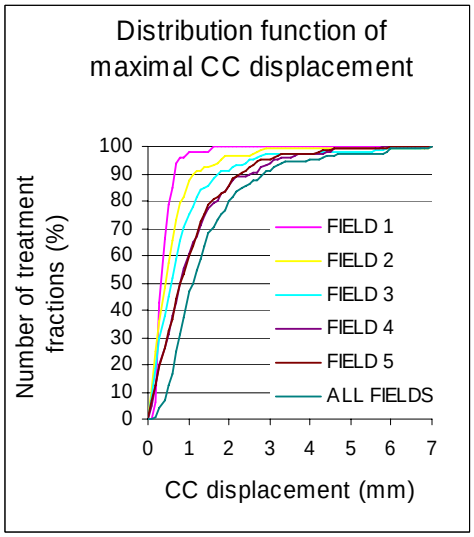

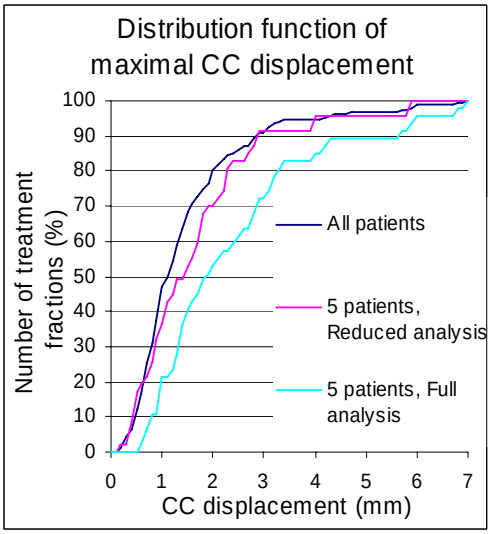

Figure 15. Shows the distribution of the maximum prostate displacement for all fractions (196 fractions) in all fields or in each field separately. (Field 1: 47 fractions, Fields 2-5: 196 fractions. **Figure 16.** compares the reduced analysis to the full analysis.

In figures 15 and 16 the x-axis represents the displacement, which was divided into intervals of 0.1 mm. The total number of treatment fractions in a specific displacement interval (for example 0-2.3 mm) is then presented in percentage of the total number of treatment fractions (196 fractions). The results of the calculations are visualized in a plot showing the number of treatment fractions in percentage against the CC displacement in mm. The same type of calculations was made for each field separately so that they could be compared to each other and to all the fields as a total. There was a restriction in the calculations of the plot for field 1: this calculation included only 47 fractions, as opposed to the other fields which included a calculation of 196 fractions. The reason for this difference is that the reduced analysis did not give any information about the prostates gland's displacement in field 1 (see CC analysis p.11). For this reason, the calculations of field 1 included less information and less significant statistics.

Tabel 1. Results from figure 15

Field	85%	90%	95%	100%
1	<0.6 mm	<0.7 mm	<0.8 mm	<1.6 mm
2	<1.0 mm	<1.1 mm	<1.8 mm	<6.9 mm
3	<1.4 mm	<1.7 mm	<2.4 mm	<6.8 mm
4	<2.0 mm	<2.5 mm	<3.2 mm	<5.8 mm
5	<1.9 mm	<2.2 mm	<2.7 mm	<6.0 mm
Total	<2.4 mm	<2.9 mm	<4.1 mm	<6.9 mm

In fields 4 and 5 a margin of 9 mm was satisfying to compensate for the prostate gland intrafractional motion in the CC direction. In 95 % of all fractions the motion was < 4.1 mm. In fields 2 and 3 the motion of the prostate gland was < 2.4 mm in 95 % of all fractions. In field 1 a margin of 9 mm was unnecessary because the prostate gland motion was < 0.8 mm in 95 % of all fractions and < 2 mm in 100 % of all fractions. This is because of the short time between the completion of the set up and the start of the beam. In this short time the prostate gland did not move far from its start position. The margin of 9 mm in the CC direction also takes into account the systematic errors (occurring from delineation errors, the treatment modalities as sag in accelerator and OBI system, misalignment of the laser system and so on) and set-up errors. The result above is just one of the three errors that PTV compensates for, and in order to reduce the margin an extended analysis including all three errors is necessary. In figure 16 the full and the reduced analysis were compared using the results from the five patients that were included in the full analysis. The calculations were made and visualized in the same way as in figure 15. An observation from figure 16 is that the curve representing the reduced analysis is steeper than the curve representing the full analysis. This is because the maximum deviation of the prostate gland in each fraction usually did not occur in the first image in each sequence. The full analysis included more measurements which contains bigger variations. The time elapse during gantry rotation was approximately 1 min and the total fraction time was approximately 5 min. Most of the deviation occurred between the fields when the beam was off which is visible in figures 12 and 13. The intrafield motion is small compared to the intrafraction motion.

PA-analysis

The PA analysis (full analysis) included a study of the CINE picture sequence of field 1 from the recorded fractions. The outcome of this analysis was that the prostate gland motion in the LT direction was < 1 mm in all fractions except in one fraction where the maximum motion was 1.32 mm (Figure 17). This can be interpreted as no significant motion in the LT direction. To make this assumption from data that only contains information of field 1 during sequences of 10 s could be uncertain since the prostate gland did not have time to deviate far from its start position. But this result makes it possible to make an assumption that the motion of the prostate gland was small and did not affect the calculation of the AP motion. The calculation of the PA motion is only an estimation because there was no possibility to calculate the start position of the prostate in field 1. In figure 19 it is possible to see the estimated PA motion. There is no information of the start position in field one so an offset is added to the PA coordinates to make it easier to visualize the connection between the two motions. Considering this the results from this analysis can only be used as guidelines for further investigations. However, as shown in figures 18 and 19, the expected result of the PA motion was obtained. In figures 18 and 19 it is shown that there is a connection between PA motion and CC motion and that the direction of the total motion is a combination of these two. The squared correlation factor was calculated for one patient in figure 18 and the result was 0.75 which indicated that there is a good correlation between anterior-cranial directions.

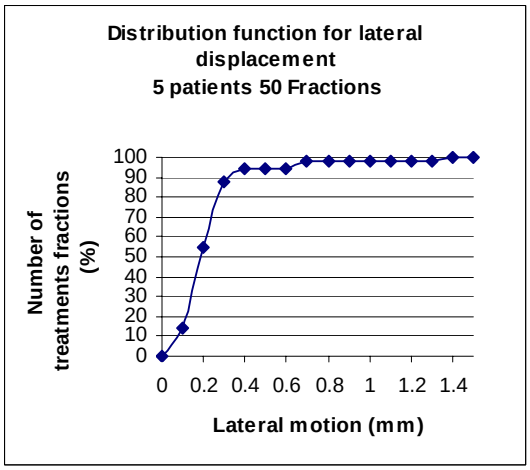

Figure 17. The analysis of lateral displacement for field 1 in the full analysis.

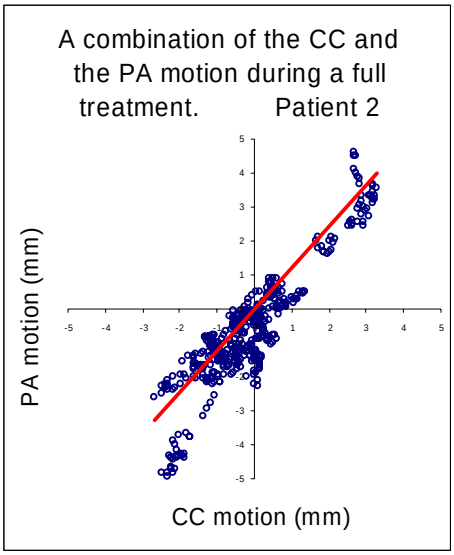

Figure 18. PA and CC motion in the same plot shows the prostate gland's motion during a whole treatment.

The margin used in treatment planning in the LT direction was 5 mm and the results from the analysis of the PA field (5 patients, 50 fractions) show that all fractions had movements < 1.4 mm. To reduce the margin it is necessary to make a larger investigation including the five fields and take a look at the procedures that occur before the treatment as planning CT, treatment set-up and so on. A group of five patients as included in this analysis may not be representative for the prostate gland's motion in all prostate cancer patients and it would be more statistically significant if the analysis included a larger cohort before reducing the LT margin.

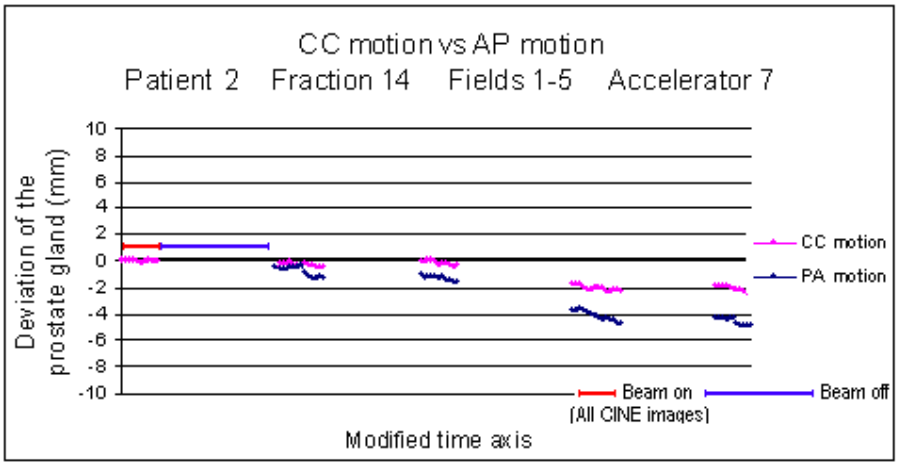

Figure 19. A typical appearance of a plot with the two motions in the same coordinate system.

In the fractions where the motion was extremely large (> 6 mm) gas was observed in the rectum. The gas appeared as a dark cloud in the CINE picture sequence and it was possible to see how the gas cloud pushed the prostate gland several mm from its start position. This gas cloud passed through very quickly and the prostate gland returned to its start position after a few seconds. The margins used today take this kind of motion into account. But what if the margin was reduced and the prostate came outside of the margin for just a moment? Would this affect the outcome of the treatment? If not, how much of the prostate gland can be outside of the margin and for how long, without affecting the outcome? To answer these questions, further research is necessary.

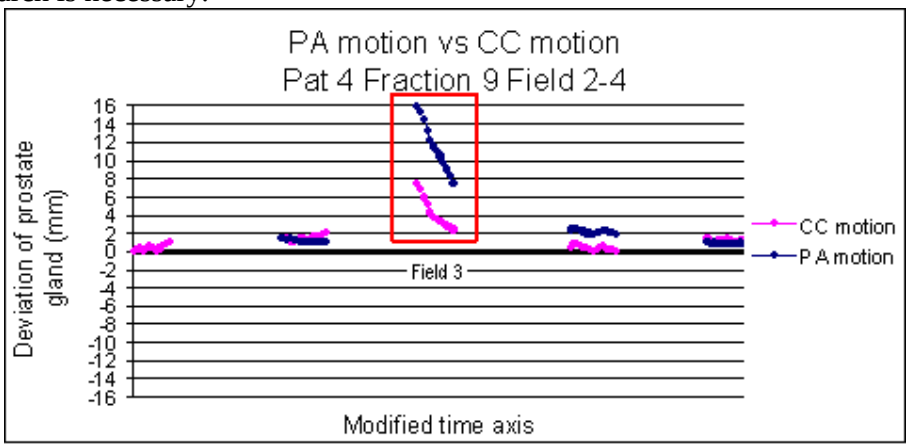

Figure 20. The results of the full analysis of an extreme case. Both CC motion and PA motion are visualized.

Figure 20 shows an extreme case where it is probable that one or two gold seed markers were placed in the rectum wall and not in the prostate gland. It is important to detect this type of misplacements at an early stage in order to obtain the best outcome of the treatment. In Århus there are standard procedures for this. In this particular case a new set of markers should have been inserted and a new CT scan performed. If the markers are misplaced the prostate gland could end up in the wrong position during the set up procedure which could lead to incomplete treatment of the prostate gland. In field 3 there was an extreme motion (fig 20) due

to gas passing through in the rectum. In the CINE picture sequence the three markers were pushed several mm in both the CC direction and PA direction (fig 21).

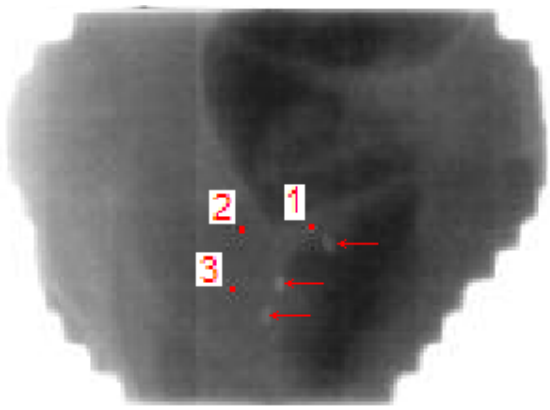

Figure 21. The red marks represent the start position and the red arrows point at the stop position. When looking closer at the three markers, it was possible to see that marker 1 had moved a shorter distance than the other markers. This might be caused by misplacement of the marker. In the background there is a black gas cloud in the rectum.

Investigations of a common pattern

Table 2. Patients with large observed movements.

	In fractions 2, 3 or 4	Not in fractions 2, 3 or 4
In fractions 9, 14, 19, 24, 29, 34 or 39	8	4
Not in fractions 9, 14, 19, 24, 29, 34 or 39	3	5

In order to see if it was possible to draw conclusions on basis of the motion of the prostate gland during fractions 2, 3 and 4 of the rest of the treatment (36 fractions) the fractions were divided into 4 groups.

The 4 groups were divided on basis of when a motion exceeding 3 mm occurred.
Group 1. Motion in one of the fractions 2, 3 or 4 and in one of the fractions 9, 14, 19, 24, 29, 34 or 39
Group 2. Motion in one of the fractions 2, 3 or 4 and no motion in the fractions 9, 14, 19, 24, 29, 34 or 39
Group 3. No motion in the fractions 2, 3 or 4 but motion in one of the fractions 9, 14, 19, 24, 29, 34 or 39
Group 4. No motion in the fractions 2, 3 or 4 and no motion in the fractions 9, 14, 19, 24, 29, 34 or 39

To check if there was a possibility to use the fractions 2, 3 and 4 to predict large motions in the rest of the fractions the sensitivity and a specificity of the method were calculated.

Sensitivity = p (In fractions 2, 3 or 4| In fractions 9, 14, 19, 24, 29, 34 or 39)
Specificity=p (Not in fractions 2, 3 or 4| Not in fractions 9, 14, 19, 24, 29, 34 or 39)

Sensitivity =67%
Specificity=63%

The results in table 2 show that the motion occurred randomly and that the accuracy is too low to predict if there is a motion or not in a late stage of a treatment just using the fractions 2, 3 and 4. In only approximately 2 out of 3 cases a correct prediction is made.

Conclusions

There was no motion > 7.0 mm in the CC-direction and in the total of 196 fractions that were included in this study 95 % had a maximum motion < 4.1 mm.

The maximum deviation in the CC direction of each field increased up to field 4 and then it looks like a steady state is reached. The maximum deviation in each fraction was most common in the interval 0.5-1.5 mm in caudal direction and occurred in approximately 40 % in field 4.

It was clearly shown that in most cases the intrafield motion was < 1 mm compared to the intrafraction motion which could be up to several mm in the CC-directions. In the AP direction it is assumed that the same conclusion of the intrafield and the intrafraction motion could be applied.

The full analysis of the CC motion and the estimation of the AP motion suggest a correlation in the anterior-cranial direction. But it could only be used as a guideline and is not to be used to reduce margins in the AP direction.

Extreme motion is often seen in connection with gas in the rectum.

The investigation of if there is a common pattern in prostate motion that could describe a whole treatment gives the conclusion that the larger motion of the prostate gland is impossible to predict, and the motion occurs randomly. Only two thirds are predicted correctly which is not good enough to be used clinically.

Acknowledgment

First, I would like to thank my supervisors Henriette Honoré and Per Rugård Poulsen, Århus University Hospital, for their excellent support during the past 20 weeks. I am very grateful for the time they have spent helping me, in spite of the fact that they had very busy schedules. I would also thank Tommy Knöös who made the contact with Henriette Honoré in Århus, which made this project possible to carry out.

I would also like to thank all the staff at the department of medical physics, Århus University Hospital, for letting me use theire equipment and for making me feel like one in the team.

Finally, many thanks to my family and especially to my wife Maja who has supported me all the way from Malmö to Århus and for her assistance in making this report readable.

References

1. www.welchcancercenter.org
2. www.socialstyrelsen.se
3. www.umm.edu/prostate
4. www.prostate-cancer-radiotherapy.org.uk Professor Les Bradbury

ImageJ

5. http://rsb.info.nih.gov/ij/

Conformal radio therapy, organ motion and side effects:

6. Dearnaley, D.P.; Khoo, V.S.; Norman, A.R.; Meyer, L.; Nahum, A.; Tait, D.; Yarnold, J.; Horwich, A. Comparison of radiation side-effects of conformal and conventional radiotherapy in prostate cancer: a randomised trial. Lancet (British edition) 1999: 353: 9149: 267-272
7. Happersett, L.; Mageras, G.S.; Zelefsky, M.J.; Burman, C.M.; Leibel, S.A.; Chui, C.; Fuks, Z.; Bull, S.; Ling, C.C.; Kutcher, G.J. A study of the effects of internal organ motion on dose escalation in conformal prostate treatments. Radiotherapy and Oncology. 2003: 66: 3: 263-270

Escalation risks:

8. Kuban, D.; Pollack, A.; Huang, E.; Levy, L.; Dong, L.; Starkschall, G.; Rosen, I. Hazards of dose escalation in prostate cancer radiotherapy. International Journal of Radiation Oncology*Biology*Physics: 2003: 57: 5: 1260-1268

Dose escalation info:

9. Zelefsky, M.J.; Chan, H.; Hunt, M.; Yamada, Y.; Shippy, A.M.; Amols, H. Long-Term Outcome of High Dose Intensity Modulated Radiation Therapy for Patients With Clinically Localized Prostate Cancer. Journal of urology: 2006: 176: 4: 1415-1419
10. Cheung, R.; Tucker, S.L.; Lee, A.K.; de Crevoisier, R.; Dong, L.; Kamat, A.; Pisters, L.; Kuban, D. Dose-response characteristics of low- and intermediate-risk prostate cancer treated with external beam radiotherapy. International Journal of Radiation Oncology*Biology*Physics: 2005: 61: 4: 993-1002
11. Brabbins, D.; Martinez, A.; Yan, D.; Lockman, D.; Wallace, M.; Gustafson, G.; Chen, P.; Vicini, F.; Wong, J. A dose-escalation trial with the adaptive radiotherapy process as a delivery system in localized prostate cancer: Analysis of chronic toxicity. International Journal of Radiation Oncology*Biology*Physics: 2005: 61: 2: 400-408

Marker info:

12. Litzenberg, D.; Dawson, L.A.; Sandler, H.; Sanda, M.G.; McShan, D.L.; Ten Haken, R.K.; Lam, K.L.; Brock, K.K.; Balter, J.M. Daily prostate targeting using implanted radiopaque markers. International Journal of Radiation Oncology*Biology*Physics: 2002: 52: 3: 699-703

13. Kitamura, K.; Shirato, H.; Shimizu, S.; Shinohara, N.; Harabayashi, T.; Shimizu, T.; Kodama, Y.; Endo, H.; Onimaru, R.; Nishioka, S.; Aoyama, H.; Tsuchiya, K.; Miyasaka, K. Registration accuracy and possible migration of internal fiducial gold marker implanted in prostate and liver treated with real-time tumor-tracking radiation therapy (RTRT). Radiotherapy and Oncology: 2002: 62: 3: 275-281

14. Pouliot, J.; Aubin, M.; Langen, K.M.; Liu, Y.-M.; Pickett, B.; Shinohara, K.; Roach, M. (Non)-migration of radiopaque markers used for on-line localization of the prostate with an electronic portal imaging device. International Journal of Radiation Oncology*Biology*Physics: 2003: 56: 3: 862-866

Prostate motion:

15. Byrne, T.E. A review of prostate motion with considerations for the treatment of prostate cancer. Medical Dosimetry: 2005: 30: 3: 155-161

Allternative visualization techniques:

16. Ciernik, I.F.; Baumert, B.G.; Egli, P.; Glanzmann, C.; Lutolf, U.M. On-line correction of beam portals in the treatment of prostate cancer using an endorectal balloon device. Radiotherapy and Oncology: 2002: 65: 1: 39-45

17. Carl, J.; Lund, B.; Larsen, E.H.; Nielsen, J. Feasibility study using a Ni-Ti stent and electronic portal imaging to localize the prostate during radiotherapy. Radiotherapy and Oncology: 2006: 78: 2: 199-206

18. Bergstrom, P.; Lofroth, P.-O.; Widmark, A. High-precision conformal radiotherapy (HPCRT) of prostate cancer-a new technique for exact positioning of the prostate at the time of treatment - Results of a dose escalation study. International Journal of Radiation Oncology*Biology*Physics: 1998: 42: 2: 305-311

19. McNair, H.A.; Parker, C.; Hansen, V.N.; Askew, L.; Mukherjee, R.; Nutting, C.; Norman, A.R.; Dearnaley, D.P. An Evaluation of Beam Cath(R)in the Verification Process for Prostate Cancer Radiotherapy .Clinical Oncology: 2004: 16: 2: 138-147

Appendix 1

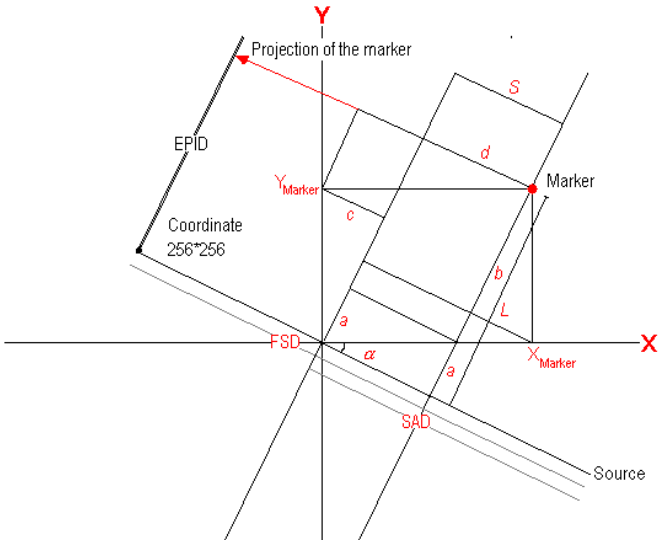

$G =$ Gantry $\qquad \alpha =$ G-90°

$X_{EPID} =$ X coordinate in EPID system $\qquad Corr =$ Correction factor

$SAD = 100\ cm \qquad FSD = 150\ cm$

$f =$ Magnification factor $\qquad X_{Mar\,ker} =$ Room coordinate

$Y_{Mar\,ker} =$ Room coordinate

$L = a + b \qquad a = X_{Mar\,ker} \cdot \sin\alpha \qquad b = Y_{Mar\,ker} \cdot \cos\alpha$

$S = d - c \qquad d = X_{Mar\,ker} \cdot \cos\alpha \qquad c = Y_{Mar\,ker} \cdot Sin\alpha$

Equation.1 describes the magnification from the iso centre plane to the EPID's plane.

$$X_{EPID} = -\frac{FSD}{SAD - S} \cdot L = -\frac{FSD}{SAD - \left(X_{Mar\,ker}\cos\alpha - Y_{Mar\,ker\,e}\sin\alpha\right)} \cdot \left(X_{Mar\,ker}\sin\alpha - Y_{Mar\,ker}\cos\alpha\right)$$

Equation.2

$$G = 180^{\circ} \Rightarrow \alpha = 90^{\circ} \qquad X_{EPID} = -\frac{FSD \cdot X_{Mar\,ker}}{SAD + Y_{Mar\,ker}} \qquad \frac{dX_{EPID}}{dY} \approx -\cos\alpha \Rightarrow dy \approx -\frac{dX_{EPID}}{\cos\alpha}$$

Equation.3 is the generally equation with two unknown variables X_{Marker}, Y_{Marker}.

$$X_{EPID} = 256 + Corr - \frac{\frac{FSD}{f} \cdot \left(X_{Mar\,ker}\sin\alpha + Y_{Mar\,ker}\cos\alpha\right)}{SAD - \left(X_{Mar\,ker}\cos\alpha - Y_{Mar\,ker}\sin\alpha\right)}$$

Euqation.4 is the definition of X_{Marker} for field one ($\alpha = 90$).

$$X_{EPID}^{180} = 256 + Corr - \frac{\frac{FSD}{f}\cdot X_{Mar\,ker}}{SAD + Y_{Mar\,ker}} \Rightarrow \qquad X_{Mar\,ker} = \left(X_{EPID}^{180} - 256 - Corr\right)\left(SAD + Y_{Mar\,ker}\right)\cdot\frac{f}{FSD}$$

Equation.5 is the simplified eq.3 with eq.4 inserted.

$$X_{EPID}^{\alpha} - 256 - Corr = \frac{SAD\cdot\sin\alpha + Y_{Mar\,ker}\cdot\sin\alpha - \frac{FSD\cdot\cos\alpha\cdot Y_{Mar\,ker}}{f\left(X_{EPID}^{180} - 256 - Corr\right)}}{\frac{SAD}{\left(X_{EPID}^{180} - 256 - Corr\right)} + \frac{SAD}{FSD}\cdot f\cdot\cos\alpha + \frac{f}{FSD}\cdot Y_{Mar\,ker}\cdot\cos\alpha + \frac{Y_{Mar\,ker}\cdot\sin\alpha}{\left(X_{EPID}^{180} - 256 - Corr\right)}}$$

Equation.6 is the equation that defines the variable Y_{Marker}

$$Y_{Mar\,ker} = \frac{SAD\cdot\frac{\left(X_{EPID}^{\alpha} - 256 - Corr\right)}{\left(X_{EPID}^{180} - 256 - Corr\right)} + \frac{f\cdot\cos\alpha}{FSD}\cdot\left(X_{EPID}^{\alpha} - 256 - Corr\right) - \sin\alpha}{\sin\alpha - \frac{\cos\alpha\cdot FSD}{f\left(X_{EPID}^{180} - 256 - Corr\right)} - \frac{f}{FSD}\cdot\cos\alpha\left(X_{EPID}^{\alpha} - 256 - Corr\right) \pm \sin\alpha\cdot\frac{\left(X_{EPID}^{\alpha} - 256 - Corr\right)}{\left(X_{EPID}^{180} - 256 - Corr\right)}}$$

Appendix 2 Exampels of a full treatment of one patient. Showing the AP and the CC motion in field 1, 2, 3 and 4.

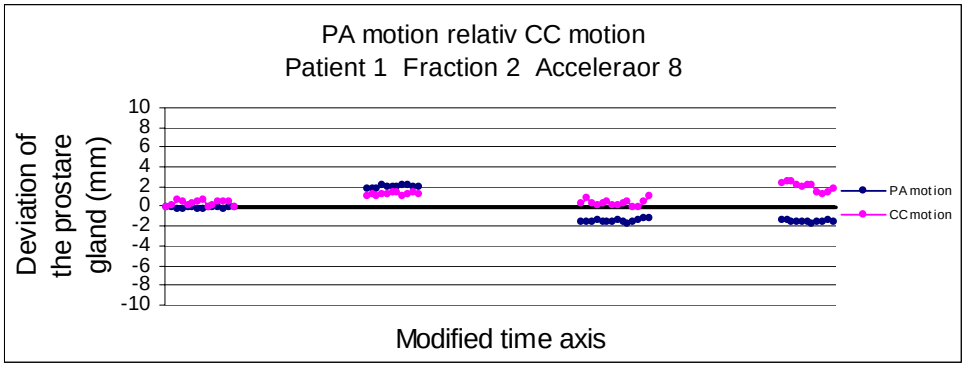

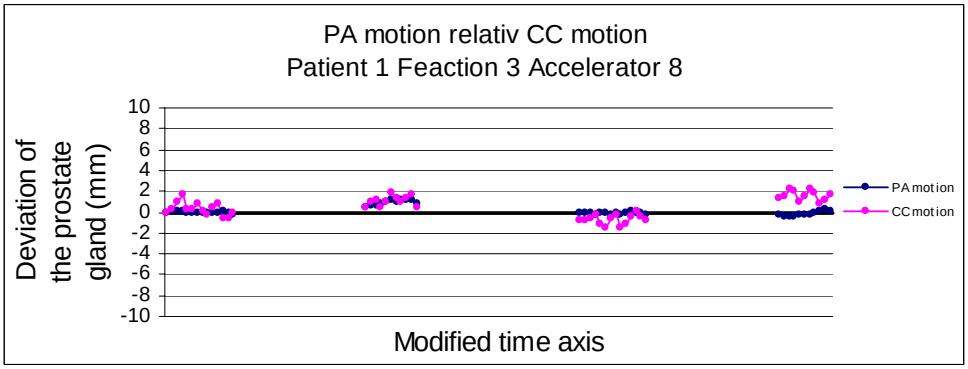

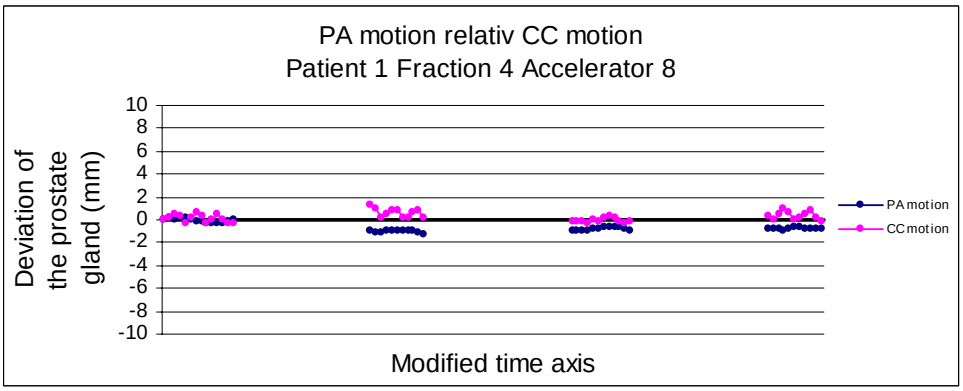

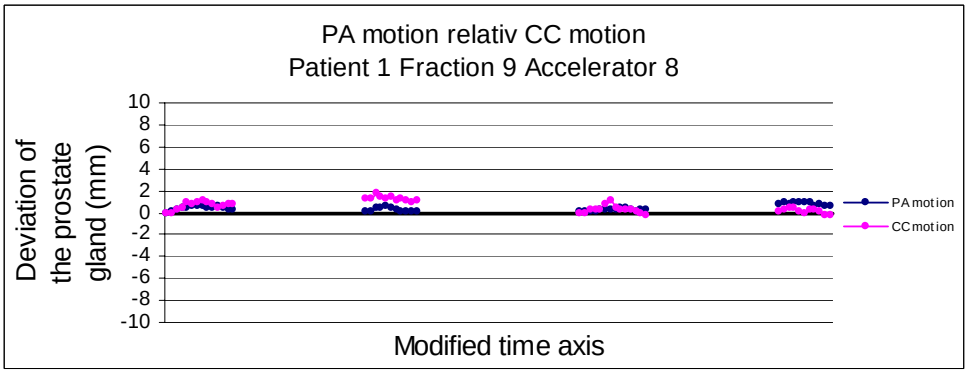

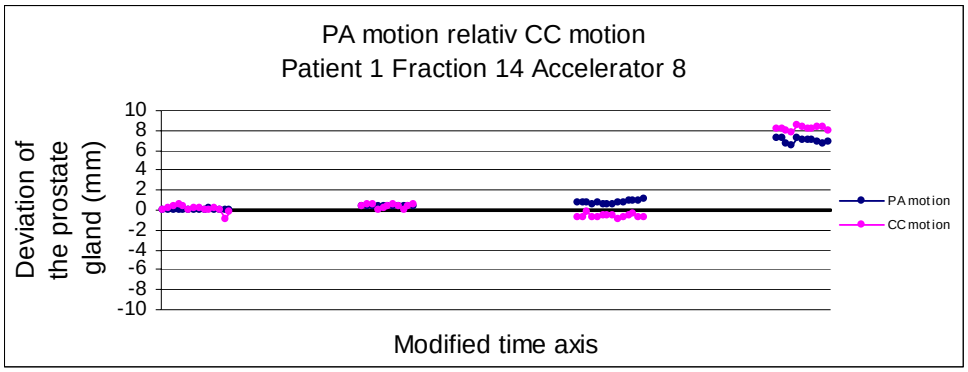
PA motion relativ CC motion
Patient 1 Fraction 14 Accelerator 8
Deviation of the prostate gland (mm)
10
8
6
4
2
0
-2
-4
-6
-8
-10
PA motion
CC motion
Modified time axis

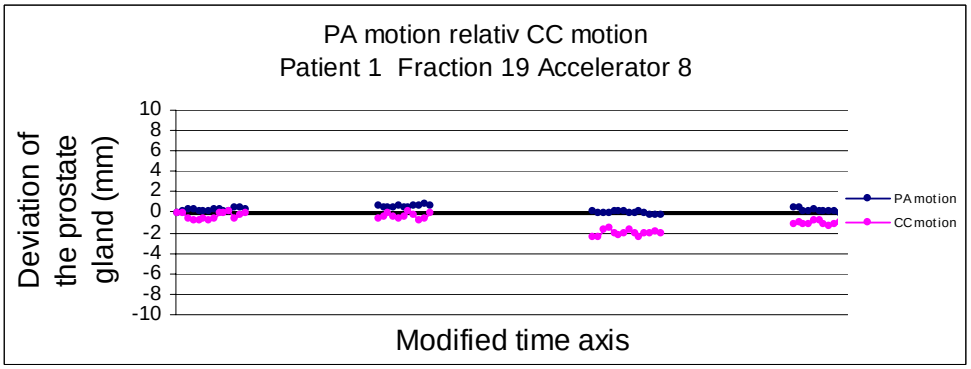
PA motion relativ CC motion
Patient 1 Fraction 19 Accelerator 8
Deviation of the prostate gland (mm)
10
8
6
4
2
0
-2
-4
-6
-8
-10
PA motion
CC motion
Modified time axis

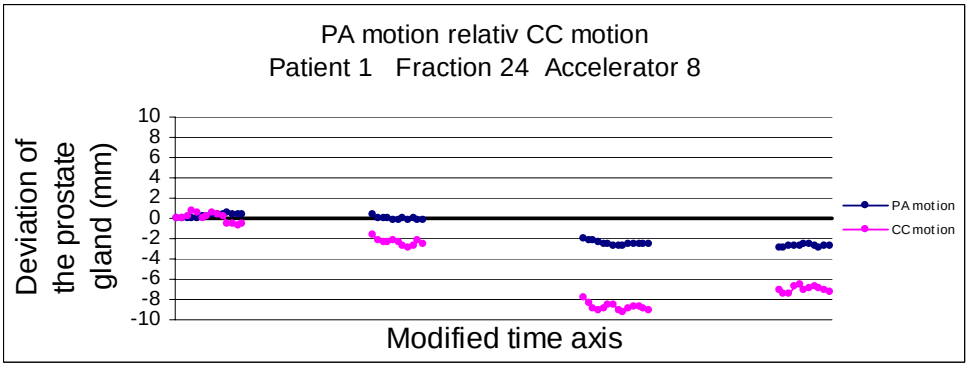
PA motion relativ CC motion
Patient 1 Fraction 24 Accelerator 8
Deviation of the prostate gland (mm)
10
8
6
4
2
0
-2
-4
-6
-8
-10
PA motion
CC motion
Modified time axis

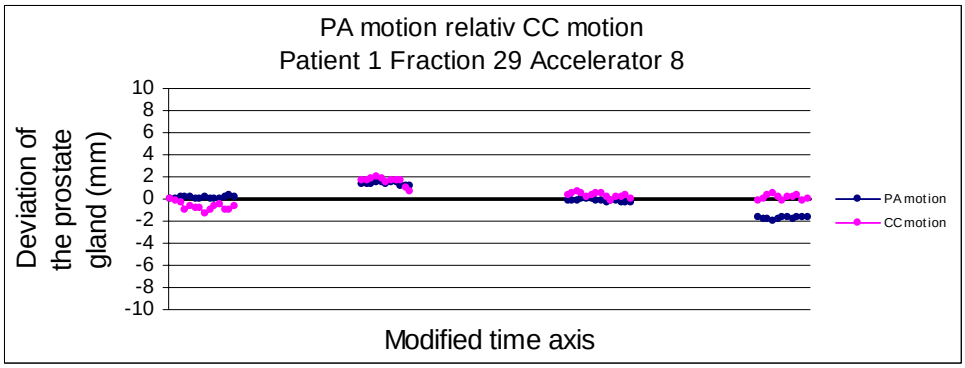
PA motion relativ CC motion
Patient 1 Fraction 29 Accelerator 8
Deviation of the prostate gland (mm)
10
8
6
4
2
0
-2
-4
-6
-8
-10
PA motion
CC motion
Modified time axis

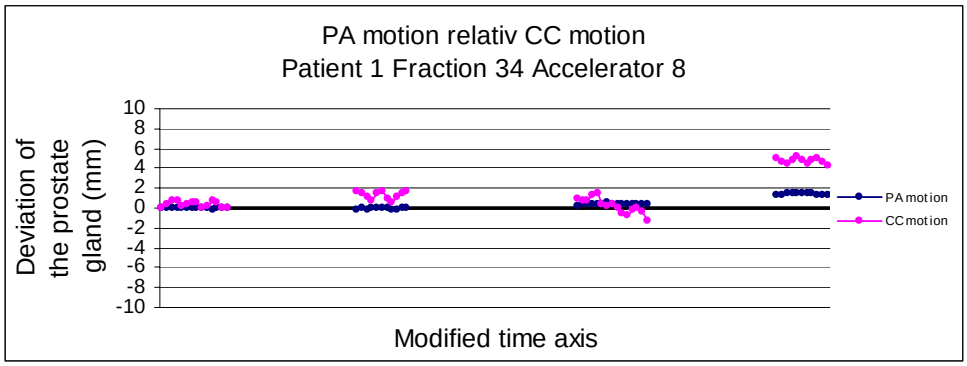
PA motion relativ CC motion
Patient 1 Fraction 34 Accelerator 8
Deviation of the prostate gland (mm)
10
8
6
4
2
0
-2
-4
-6
-8
-10
PA motion
CC motion
Modified time axis

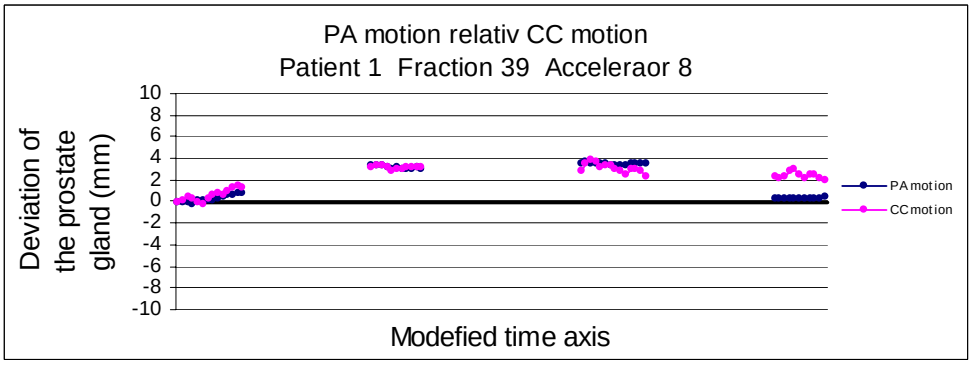
PA motion relativ CC motion
Patient 1 Fraction 39 Acceleraor 8
Deviation of the prostate gland (mm)
10
8
6
4
2
0
-2
-4
-6
-8
-10
PA motion
CC motion
Modefied time axis